Optimization of gaseous nitriding of carbon iron-based alloy based on fatigue resistance modelling

Hadrien Weil [a,b], Laurent Barrallier [a], Sébastien Jégou [a], Nancy Caldeira-Meulnotte [b], Guillaume Beck [b]

a. MSMP Laboratory - Arts et Métiers ParisTech, 2 cours des Arts et Métiers, 13617 Aix en Provence, France

b. SAFRAN Transmission Systems, 18 boulevard Louis Seguin, 92707 Colombes, France

Abstract

Gaseous nitriding of steels is a well-established thermochemical surface treatments that increases the fatigue resistance of treated parts. The present work proposes a modelling of the fatigue life as a function of the applied stress. It takes into account the hardness and compressive residual stresses that developed during nitriding. The model is suitable to help optimizing nitriding parameters by reverse modelling.

Keywords: steel, multiaxial fatigue, residual stresses, hardness, numerical modelling

1. Introduction

Fatigue resistance and mechanical capacity of engine components are of vital importance for aerospace and automotive industries. Surface engineering is then used to advantages in order to improve superficial properties, such as hardness and compressive residual stress [1, 2, 3]. Among surface treatments, thermochemical surface treatments of steel, such as nitriding, proved their efficiency against the fatigue phenomenon [4, 5].

Gaseous nitriding is based on the diffusion of nitrogen atoms through the treated surface. It involves the precipitation of nanoscale alloying element nitrides MN (M = Cr, V...) that provides an increase of hardness and the generation of compressive residual stresses [2]. For a given steel composition, nitriding parameters (time, temperature, nitriding potential) and mechanical properties can be estimated based diffusion/precipitation modelling [6, 7].

Concerning residual stresses, existing models based on phase transformations allow to obtain profiles consistent with experimental data [6, 8, 9]. However, models that calculate hardness profiles such as Horàk [10] or Hiraoka [11] are only based on the diffusion phenomenon and thus cannot describe precipitation growth/coarsening effects on hardness. That is why a new model for calculating the hardness as function of the volume fraction of the different nitride populations was set up during this study.

The residual stresses and hardness can be taken into account in the fatigue lifetime calculations thanks to multiaxial fatigue criteria [12]. A comparison with fatigue tests on nitrided material allows to validate the model used. Moreover, this study adds a new possibility to optimize nitriding parameters for a given mechanical loading by reverse modelling.

2. Modelling of fatigue

Gaseous nitriding is based on the diffusion of nitrogen atoms and microstructural modifications within the depth of the treated part. It is then essential to take into account the gradient of mechanical properties (hardness, residual stresses) on the mechanical behaviour of the nitrided surface to applied stresses in order to identify the critical region for crack initiation. Thanks to preexisting multiaxial fatigue criteria and the assumptions made, a model of fatigue computation in adequacy with the mechanical properties brought by gaseous nitriding process was developed during this study.

2.1. The Dang Van criterion

The Dang Van criterion, EDV [13], allows to calculate the theoretical fatigue limit in-depth profiles for a given load, probability of failure and core hardness at each depth z and time t over a period T :

$$E_{DV}(z) = Max_{t\in T}\left(\frac{\tau(z,t) + \alpha_{DV}(N)P_H(z,t)}{\beta_{DV}(N)}\right) \quad (1)$$

The criterion uses the hydrostatic pressure P_h and the Tresca stress $\tau(z,t)$ that is a function of eigenvalues of the stress tensor as follows :

$$\tau(z,t) = \frac{1}{2}Max\left(\mid \sigma_1(z,t) - \sigma_2(z,t) \mid, \mid \sigma_2(z,t) - \sigma_3(z,t) \mid, \mid \sigma_3(z,t) - \sigma_1(z,t) \mid\right) \quad (2)$$

The hydrostatic pressure is an addition of the applied and residual stresses, $\underline{\sigma}_{\text{app}}(z,t)$ and $\underline{\sigma}_{\text{R}}(z,t)$ respectively, in the nitrided layer [12, 14, 15] :

$$P_{\text{h}}(z,t) = \frac{1}{3} tr(\underline{\sigma}_{\text{app}}(z,t) + \underline{\sigma}_{\text{R}}(z,t)) \tag{3}$$

The coefficients of the criterion $\alpha_{DV}(N)$ and $\beta_{DV}(z,N)$ must be calculated with a given number of cycles and probability of failure [12].

The fatigue limit is finally obtained when $E_{DV}(z) = 1$ (figure 1) at a given depth z, for given number of cycles N and probability of failure p.

2.2. Assumptions

Some assumptions are made for the calculations of the fatigue life :

— In the case of this study, the speed of rotation of the gears causes a large number of cycles to neglect the crack propagation phase. That is why, we are interested in crack initiation in the number of high cycles between 10^4 and 10^7.

— The coefficient $\beta_{DV}(z,N)$ takes into account the hardness $HV(z)$ at a given depth z induced by nitriding. Deperrois demonstrated that the increase in hardness has a strong influence on the coefficient β_{DV} [16]. Indeed, the coefficient becomes greater with the increase in the hardness of the material. It can be calculated using the Deperrois model :

$$\beta_{DV}(z,N) = \beta_0 \left(\frac{HV(z)}{HV_0} \right)^n \tag{4}$$

where β_0 and HV_0 are the coefficient and the hardness of the core material respectively. The coefficient n was equal to $1/2$. Indeed, in the case of nitriding, this value allows better calibration of the calculation of the limit in fatigue.

— In order to simplify the calculation, Chaussumier assumed that the coefficient $\alpha_{DV}(N)$ does not depend on the depth of the nitrided layer [12]. It is thus calculated by means of the Wöhler curves of the non-nitrided material. The Wöhler curves were obtained from different load-ratio fatigue tests (rotating bending tests, $R_{\sigma 1} = -1$, and tensile tests, $R_{\sigma 2} = 0.05$) for a given failure probability :

$$\alpha(N) = \frac{3}{2} \frac{(1 - R_{\sigma 1})(1 - R_{\sigma 2})(\sigma_1^{alt}(N) - \sigma_2^{alt}(N))}{(1 - R_{\sigma 2})\sigma_1^{alt}(N) - (1 - R_{\sigma 1})\sigma_2^{alt}(N)} \tag{5}$$

where $\sigma^{alt}(N)$ is the alternating stresses from the Wöhler curve.

— The loading $\underline{\sigma}_{\text{app}}(z,t)$ undergone by the material can come from a finite element simulation for complex parts or analytical calculations using the Hertz pressure and equations of McEwen [17]. However, the variation of the elastic constants in the nitrided layer has not been taken into account yet. It is noted note that this could have an influence on the applied stress.

— In-depth stresses (applied and residual) and mechanical behaviour gradients have not been taken into account.

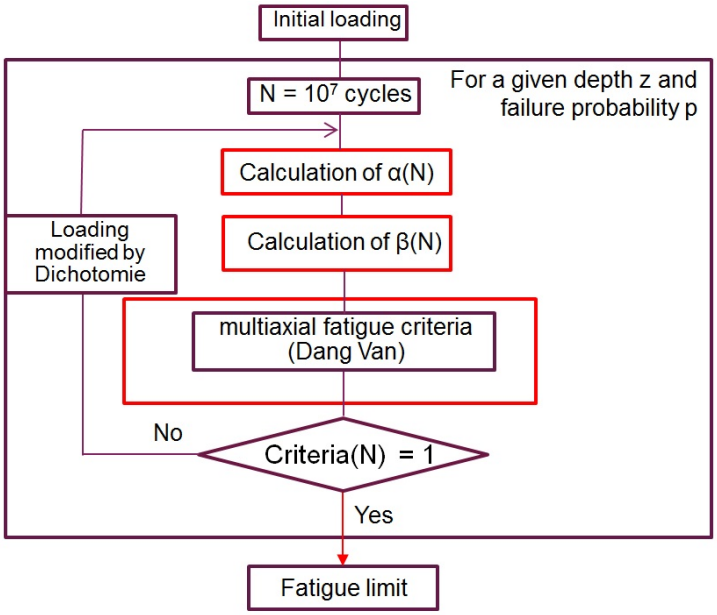

FIGURE 1: Algorithm for calculating the fatigue limit.

2.3. Influence of compressive residual stresses

The compressive residual stresses make it difficult to initiate and propagate cracks in the nitrided layer. It becomes a protective layer on the surface of the material. To model this phenomenon, the influence of compressive residual stresses on the fatigue limit of a nitrided steel is given in figure 2 for a durability of 10^7 cycles and $10^{-6}\%$ failure probability. The residual stress and loading in-depth profiles used in order to point out the effect of the mechanical properties provided by nitriding on the fatigue lifetime of a carbon iron-based alloy are given in figures 3 and 4 respectively. The residual stress is obtained by X-ray diffraction in the ferritic matrix with a Siemens

D500 and CrK_α radiation on the 2 1 1 diffracting plan. The sin^2 method is used to determine the mean stress $(\sigma_{xx} - \sigma_{zz})$. The loading is provided from simulations performed using the finite element software Ansys®. This is a result of a simulation of Hertz pressure on a tooth flank designed by Safran Transmission Systems.

The boundary surface (shown in gray in figure 2) separates the rupture zone (above) from the non-rupture zone (below). Between 0 and 250 μm depth, the probability of failure is not negligible for a material without nitriding. The presence of compressive residual stresses obviously induces a positive effect on the fatigue limit due to the decrease of the hydrostatic pressure.

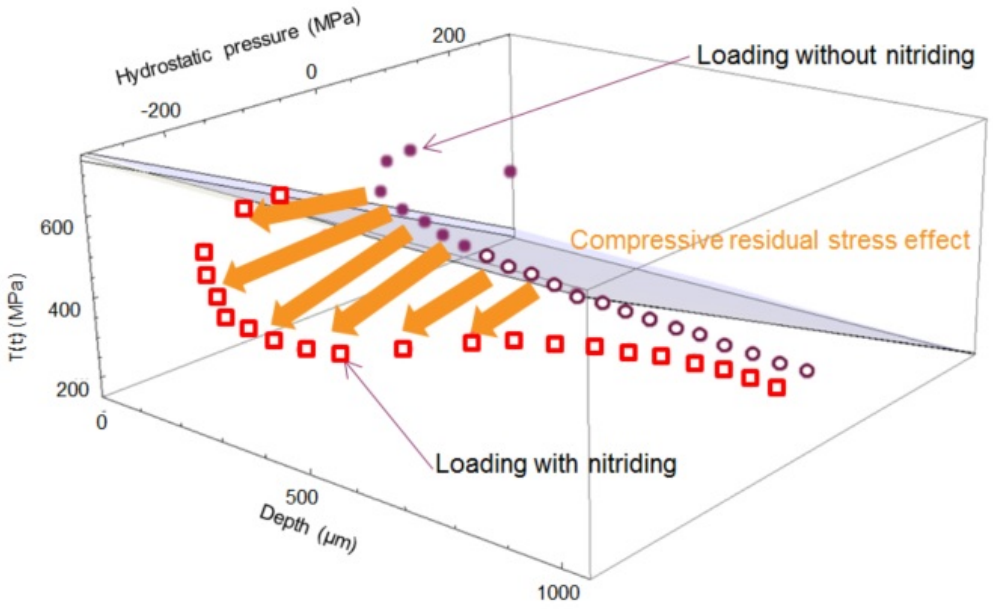

FIGURE 2: Loading with and without nitriding according to Dang Van cirterion for 10^7 cycles and $10^{-6}\%$ probability of failure. Blank and filled marks are above and below respectively the critical plane.

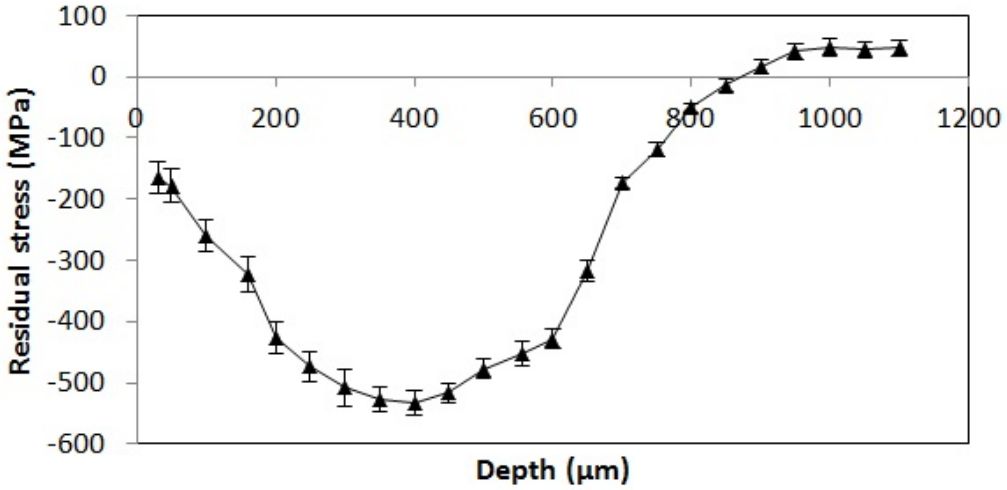

FIGURE 3: Residual stress in-depth profiles after nitriding of a carbon iron-based alloy.

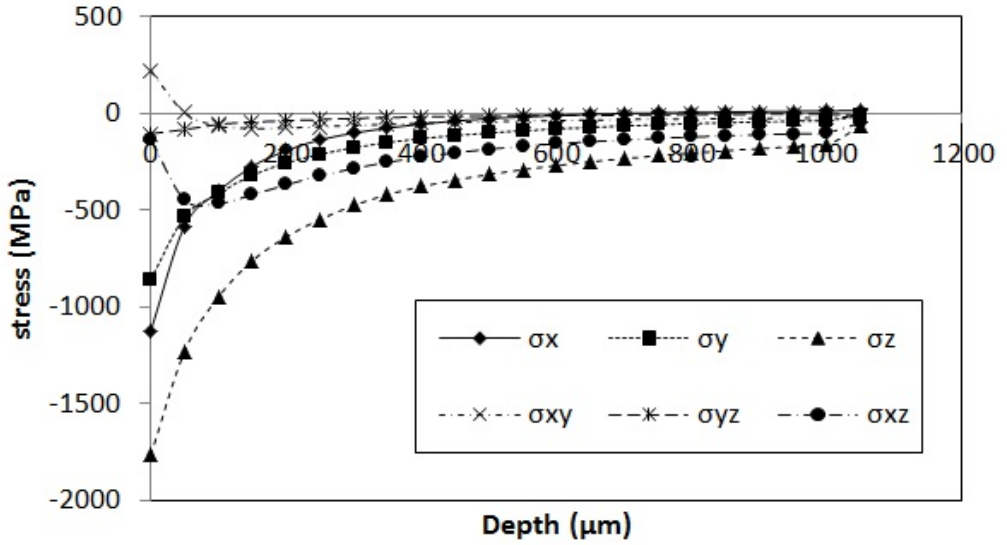

FIGURE 4: Elements of the applied stress tensor as a function of the depth in order to point out the effect of residual stresses in the fatigue limit.

2.4. Influence of the hardness

The presence of nitrides in the nitrided layer makes it possible to block the dislocations and increase the hardness. Consequently, the fatigue strength at high cycle is improved. However, the increase in hardness can weaken the layer for olygocyclic fatigue.

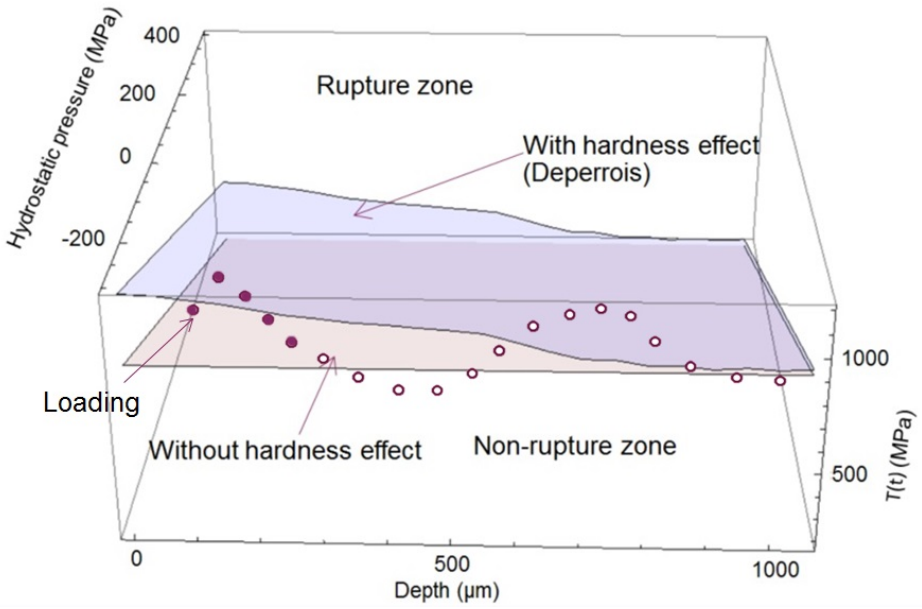

FIGURE 5: Dang Van surface with and without nitriding for 10^7 cycles and $10^{-6}\%$ probability of failure. Blank and filled marks are above and below respectively the critical plane without hardness effect.

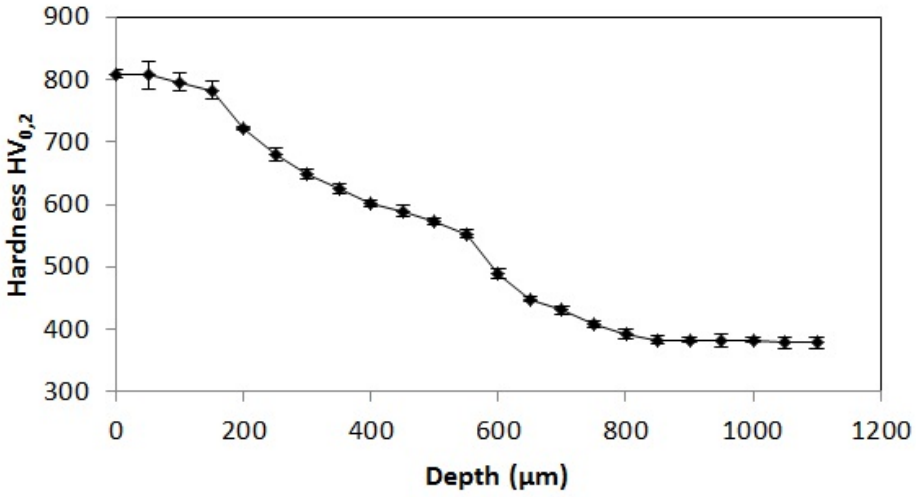

FIGURE 6: Hardness in-depth profiles after nitriding of a carbon iron-based alloy used for pointing out the influence of hardness on the fatigue limit.

Increased hardness in the nitrided layers also has a positive effect on the fatigue strength of the material (figure 5). Thanks to equation 4, the increase in the hardness makes it possible to increase the beta coefficient and it allows shifting up the boundary surface and increasing the non-rupture zone [16, 12, 15]. The hardness profile used for this calculation can be seen in figure 6. It is obtained by microdurometer Leica VMHT.

2.5. Comparison with experimental results

In order to validate the model, fatigue tests on smooth and notched specimens were carried out on a nitrided carbon iron-based alloy during this study. Tests were carried out for a frequency of 100 Hz and with censorship of 10^7 cycles.

The fatigue limit after rotational bending is found closed to 875 MPa for the notched specimen (stress concentration coefficient equal to 1,4) and 1075 MPa for the smooth specimen. The crack initiation zone depends on the specimens geometry. It takes place at the outer surface in case of the notched specimen because of the maximum stress-concentration factor as shows Figure 7. However, it takes place at the interface between the nitrided surface and the core material for smooth specimens [12].

In order to test the fatigue limit calculation approach, some simulations of rotational bending tests were carried out for smooth and notched specimens

with a reference nitriding. Simulations were set to nominal stresses of 875 MPa and 1075 MPa and performed with the Ansys software. The elements of the stress tensor resulting from the simulation are observed on the diameter of the critical zone of the specimen (figures 8). The applied stress tensor is used in calculating the fatigue limit, as well as the mechanical characteristics provided by nitriding (hardness, residual stresses in Figures 3 and 6), with a 100 μm nitrided layer rectification in order to remove the white layer on the surface. However, the geometry is not taken into account since there is no change in the diffusion of nitrogen and carbon for hardness and mechanical rebalancing for residual stresses. Results for both smooth and notched specimens are given in figure 9 for a 50% failure probability and a fatigue lifetime of 10^7 cycles which is equal to the censorship of the fatigue tests.

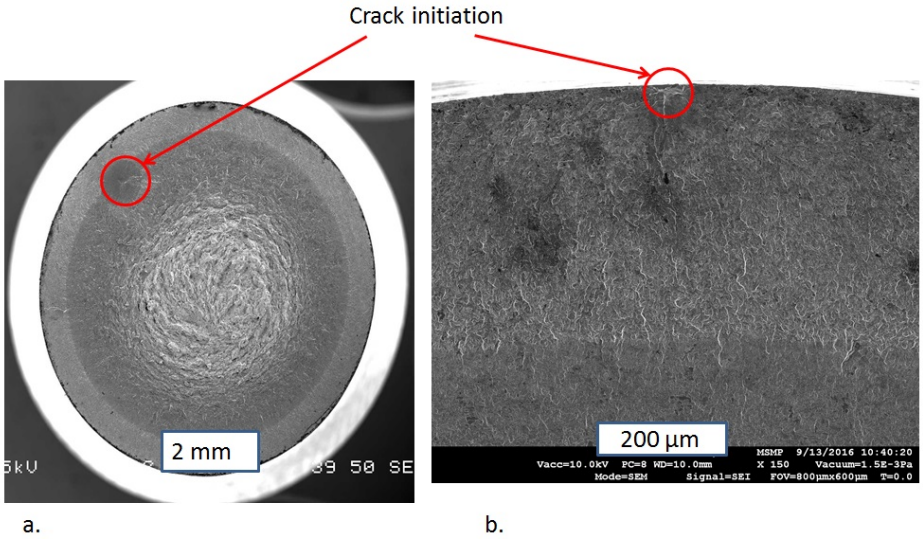

FIGURE 7: Comparison of fracture micrographs obtained by SEM for a) smooth and b) notched specimens.

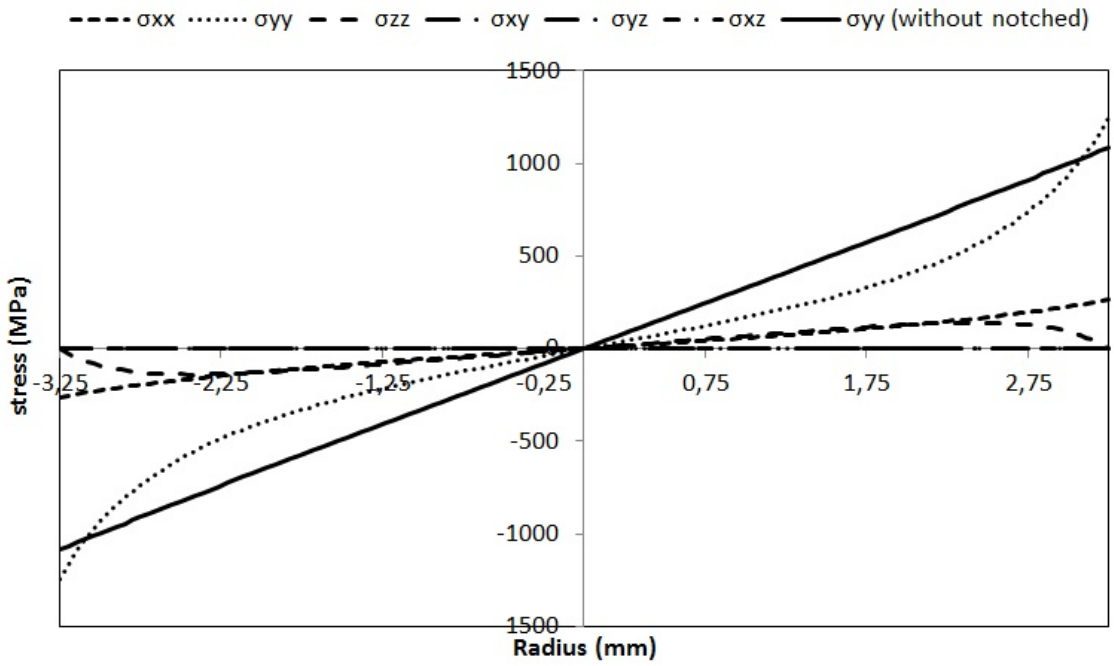

FIGURE 8: Evolution of stress tensor elements as a function of the radius for rotational bending at 875 MPa with a notched specimen and 1075 MPa for a smooth specimen (solid line).

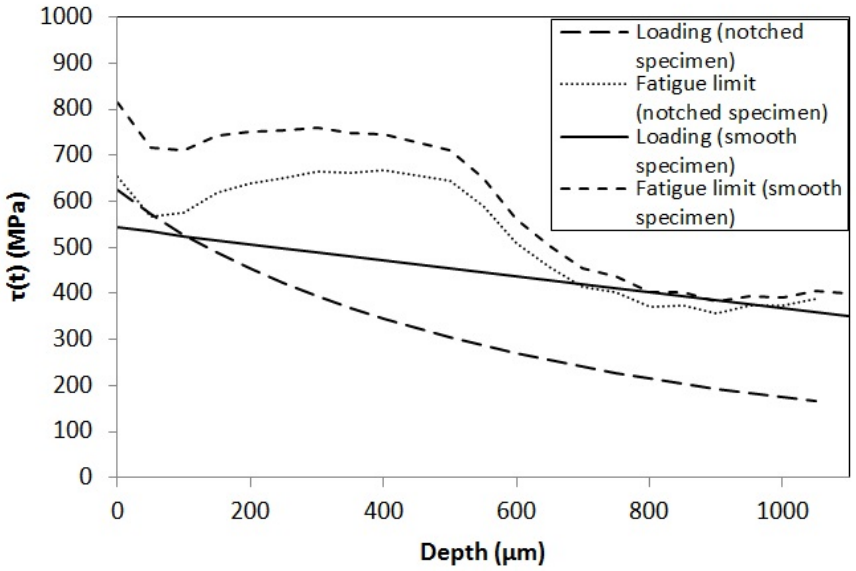

FIGURE 9: Comparison between the loading profiles from rotational bending tests and the fatigue limit of a nitrided layer calculated according to Dang Van criterion at 875 MPa for a notched specimen and 1075 MPa for a smooth specimen.

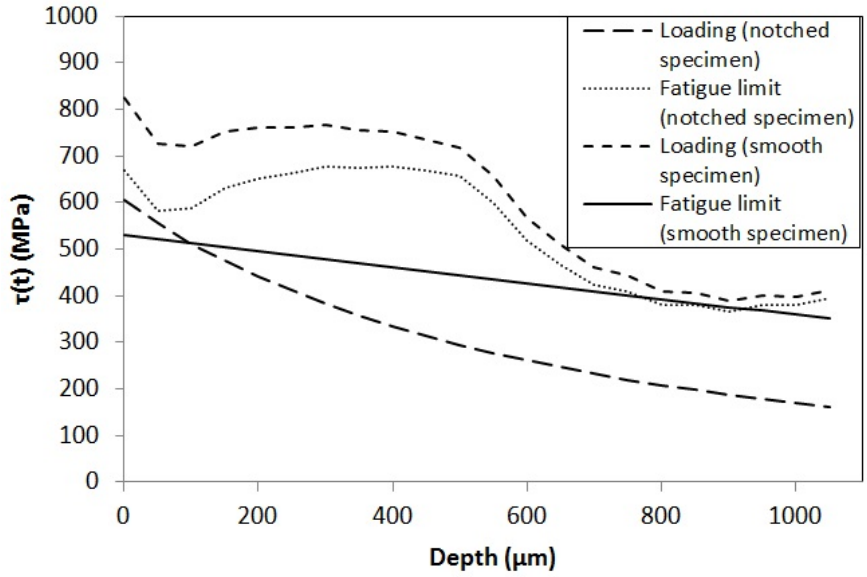

FIGURE 10: Comparison between the loading profiles from rotational bending tests and the fatigue limit of a nitrided layer calculated according to Dang Van criterion at 850 MPa for a notched specimen and 1050 MPa for a smooth specimen.

In both cases, the fatigue limit profile is superimposed with the loading at a precise location and lies in the non-break zone at other depths on figure 9. Consequently, the fatigue limit is reached with the simulation at 875 MPa for the notched specimen and 1075 MPa for the smooth specimen. The breakthrough threshold is well achieved from these two values, since at 850 MPa and 1050 MPa for notched and smooth specimens, the load is below the fatigue limit (figure 10). Indeed, the fatigue limit is reached by the loading at the end of the nitrided layer for the smooth specimen and at the beginning of the layer (the first 50 μm) for the notched specimen. The proposed model of calculation of the fatigue limit of nitrided surfaces is in good agreements with experimental observations.

3. Modelling of gas nitriding process

The algorithm used to calculate the hardness and residual stress profiles is presented in Figure 11. For each increment of time during nitriding and at each depth below the treated surface (see [6] for more details), the diffusion of carbon and nitrogen are calculated. The distribution of each phase (mass fraction and their chemical composition) is then determined by thermo-

dynamic equilibrium calculations thanks to the Thermo-Calc software [18]. Finally, the residual stress and hardness in-depth profiles are calculated.

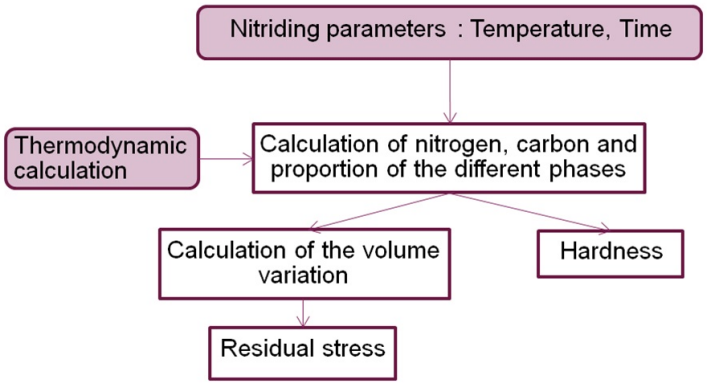

FIGURE 11: Algorithm used to model the gas nitriding process.

3.1. Calculation of residual stress

The phase volume change is calculated in order to get the volumetric eigenstrains accompanying the precipitation [19] :

$$\epsilon^{v}_{ij,p} = \frac{1}{3}\frac{\Delta V}{V}\delta_{ij} \tag{6}$$

With $\epsilon^{v}_{ij,p}$ the volumetric strain from precipitation, $\frac{\Delta V}{V}$ the volume change and δ_{ij} the symbol of Kronecker.

From the volume fraction of precipitates and calculation of the volumetric strain, the residual stress in ferrite is determined using the Kröner-Eshelby model [20]. The macroscopic stress and strain are defined as follow :

$$\begin{cases} \underline{\hat{\epsilon}} &= \underline{\hat{\epsilon}}^{e} + \underline{\hat{\epsilon}}^{l} \\ \underline{\hat{\epsilon}}^{l} &= \underline{\hat{\epsilon}}^{v} + \underline{\hat{\epsilon}}^{p} \\ \underline{\hat{\sigma}} &= \underline{C\hat{\epsilon}}^{e} \end{cases} \tag{7}$$

With $\hat{\epsilon}$ the total strain, $\hat{\epsilon}^{e}$ the elastic strain, $\hat{\epsilon}^{l}$ the stress-free strain and $\hat{\epsilon}^{p}$ the macroscopic plastic deformation.

The model assumes a two phases material defined by a ferritic matrix and an inclusion that represents all kind of precipitates. Strain in each phase is determined according to the Eshelby relation :

$$\begin{cases} \underline{\epsilon}^e_{\Phi i} &= (\underline{I}+\underline{U}).\underline{\hat{\epsilon}}^e + (\underline{I}+\underline{U}).(\underline{I}+\underline{W}^{-1}).(\underline{\hat{\epsilon}}^l - \underline{\epsilon}^l_{\Phi i}) \\ \underline{\hat{\sigma}} &= \sum_{\Phi i} y_i \underline{\sigma}_{\Phi i} \\ \underline{\hat{\epsilon}} &= \sum_{\Phi i} y_i \underline{\epsilon}_{\Phi i} \end{cases} \tag{8}$$

With $\underline{U}$ the polarization tensor to ensure the continuity of the displacements between the matrix and the precipitates, $\underline{W}$ the Eshelby tensor giving the morphology of the precipitates (spherical, ellipsoidal, etc...) and y the volume fraction of the phase ϕ. You can have more information about this approach in reading [21].

3.2. Calculation of hardness

In the context of gas nitriding, the hardness is affected by blocking dislocations with nitrides or carbides within the ferritic matrix. The Brown and Ham approach is then used to defined the hardness at a given depth z [22] :

$$HV \approx \sqrt{\tau_{cont}^2 + \tau_{cis}^2} \tag{9}$$

τ_{cont} is the stress to bypass mainly globular precipitate as given by Orowan [23] :

$$\tau_{cont} \approx \frac{\mu \cdot b \cdot {y_{\text{prec}}^{\text{globular}}}^{1/2}}{R_{\text{s}}} \tag{10}$$

With the shear modulus of the matrix μ, the modulo of the Burgers vector b, the mean radius of the precipitate in the slip plane R_{s} and the volume fraction $y_{prec}^{globular}$ of the globular.

τ_{cis} the shear stress calculated according to the volume fraction of the semi-coherent $y_{prec}^{semi-coherent}$ precipitates [24] :

$$\tau_{cis} \approx \gamma_{\text{s}}^{3/2} {R_{\text{s}}}^{1/2} {y_{\text{prec}}^{\text{semi-coherent}}}^{1/2} \tag{11}$$

With γ_{s} the interface energy between precipitate and matrix.

The hardness is finally calculated as follows :

$$HV \approx \sqrt{\left(\frac{\mu b}{R_{\text{s}}}\right)^2 y_{\text{prec}}^{\text{globular}} + \gamma_{\text{s}}^3 R_{\text{s}} y_{\text{prec}}^{\text{semi-coherent}}} \tag{12}$$

However, due to the lack of knowledge about the precipitation kinetic, the hardness is normalized according to the core and surface hardness (HV_0

and HV_s respectively) and a single factor I characterizing the influence of the two types of precipitates (incoherent and coherent) is used. That is why, the following equation was done in this study :

$$HV(z) = HV_0 + (HV_s - HV_0) \sqrt{\frac{t_{\text{eff}}}{t_{\text{eff}}} \cdot (\text{Norm}(y_{\text{prec}}^{\text{semi-cohrent}}(z)) \cdot (1 - I) + \text{Norm}(y_{\text{prec}}^{\text{globulaire}}(z)) \cdot I)} \quad (13)$$

With t_{eff} the effective time at depth z with respect to the overall nitriding time t_{eff}.

The standardized volume fraction $\text{Norm}(y_{\phi_\text{i}}(z))$ is calculated with the volume fractions of precipitates $y_{\phi_\text{i}}(z)$ at each depth z, $y_{\phi_\text{i}0}$ from the core material and $y_{\phi_\text{i}s}$ at the outter surface.

$$\text{Norm}(y_{\phi_\text{i}}(z)) = \frac{y_{\phi_\text{i}}(z) - y_{\phi_\text{i}0}}{y_{\phi_\text{i}s} - y_{\phi_\text{i}0}} \quad (14)$$

In order to calculate the volume fractions of globular and semi-coherent nitrides, it is important to dissociate the fraction from the two populations. According to the 1 :1 stoechiometry of alloying elements nitrides MN (M = Cr, V ...), and assuming a complete reaction of nitrogen with alloying elements, the fraction of nitrogen can be written as follows :

$$X_\text{N} = X_{\text{prec}} = X_{\text{Semi-coherent}} + X_{\text{Globular}} \quad (15)$$

With X_N and X_{prec} the total amount of nitrogen and nitrides and $X_{\text{Semi-coherent}}$ and X_{Globular} the amount of semi-coherent an globular nitrides respectively.

The amount of each element Z_j in a phase ϕ_i is obtained from the mass fraction of each phase W^{ϕ_i} and its chemical compositions $W_{\text{Z}_\text{j}}^{\phi_\text{i}}$.

$$X_{\text{Z}_\text{j}}^{\phi_\text{i}} = \frac{W_{\text{Z}_\text{j}}^{\phi_\text{i}} \cdot W^{\phi_\text{i}} \cdot m^{\text{tot}'}}{M_{\text{Z}_\text{j}}} \quad (16)$$

With $m^{\text{tot}'}$ the total mass after nitriding. The mass fractions of each element is determined by means of thermodynamic calculation using the Thermo-Calc software.

The calculation of the amount of nitrogen in given nitrides is carried out such as :

— The globular nitrides are formed predominantly from the initial carbides. The amount of nitrogen in semi-coherent nitrides can be obtained by subtracting the alloying elements $\mathrm{Z_j}$ from the tempered carbides $X_{\mathrm{Z_j}}^{\mathrm{carbides}}$ to the total amount of nitrogen X_{N} when $\sum_{\mathrm{Z_j}} X_{\mathrm{Z_j}}^{\mathrm{carbides}} < X_{\mathrm{N}}$:

$$X_{\mathrm{Semi-coherent}} = X_{\mathrm{N}} - \sum_{\mathrm{Z_j}} X_{\mathrm{Z_j}}^{\mathrm{carbides}} \tag{17}$$

— The semi-coherent nitrides are formed predominantly from the alloying elements contained in the ferritic matrix. The amount of globular nitrides can be obtained by subtracting the amount of elements $\mathrm{Z_{j'}}$ from the ferritic matrix $X_{\mathrm{Z_{j'}}}^{\mathrm{Fe}}$ to the amount of nitrogen X_{N} when $\sum_{\mathrm{Z_{j'}}} X_{\mathrm{Z_{j'}}}^{\mathrm{Fe}} < X_{\mathrm{N}}$:

$$X_{\mathrm{Globular}} = X_{\mathrm{N}} - \sum_{\mathrm{Z_{j'}}} X_{\mathrm{Z_{j'}}}^{\mathrm{Fe}} \tag{18}$$

The mass $W^{\phi_{\mathrm{i}}}$ and volume $Y^{\phi_{\mathrm{i}}}$ fractions of the two types nitrides are deduced from the followings :

$$W^{\phi_{\mathrm{i}}} = \frac{X^{\phi_{\mathrm{i}}} \cdot M^{\phi_{\mathrm{i}}}}{m^{\mathrm{tot'}}} \tag{19}$$

With $M^{\phi_{\mathrm{i}}}$ the molar mass of the phase ϕ_{i}.

$$Y^{\phi_{\mathrm{i}}} = \frac{W^{\phi_{\mathrm{i}}} \cdot V^{\phi_{\mathrm{i}}}}{V^{\mathrm{tot}}} \tag{20}$$

With $V^{\phi_{\mathrm{i}}}$ the massic volume of the phase ϕ_{i} and V^{tot} the total volume.

By calculating the volume fractions of globular and semi-coherent nitrides, the proposed model is applied in order to obtain the hardness in the nitrided layer.

3.3. Results

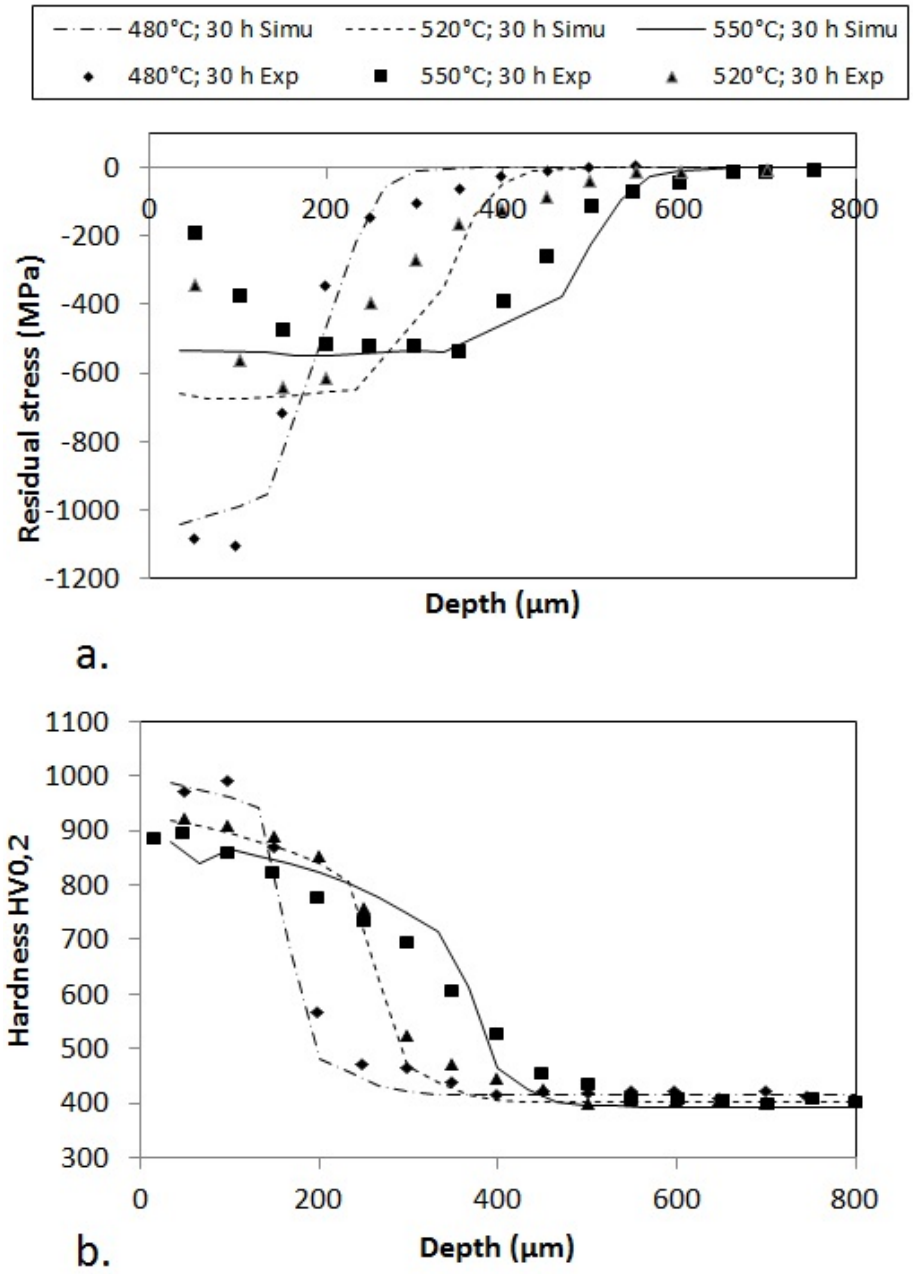

FIGURE 12: Comparisons of (a) residual stress and (b) hardness in-depth profiles obtained from simulation and experiments carried out at 480, 520 and 550°C during 30 h [25].

The residual stresses and hardness profiles from modelling are compared to experiments carried out at 480, 520 and 550°C during 30 h [25] (figure 12). The standard deviations of experimental data do not exceed 50 MPa for residual stresses and 30 HV0,2 for microhardness. Modelling and experiments are in good agreements. However, the progressive decrease of the residual stresses in the near surface, due to the kinetics of precipitation/dissolution of each phase during nitriding and the corresponding mechanical loading/unloading, has not been considered yet.

4. Application to the optimization of nitriding parameters

to close this study, a reverse modelling was set up in order to obtain hardness and residual stress limits profiles for a given failure probability, lifetime and applied stresses. The obtained profiles allow the optimization of the nitriding parameters.

4.1. Methodology

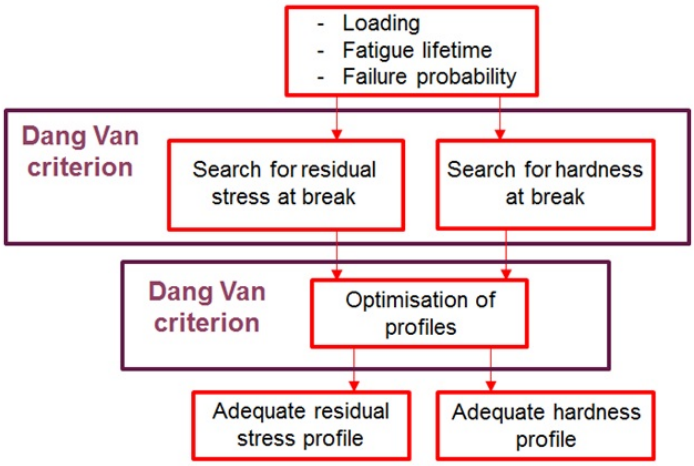

FIGURE 13: Algorithm for calculating the optimization of the requirement of residual stresses and hardness.

The proposed approach can be used in reverse modelling in order to find the minimum hardness and residual stress in-depth profiles required for a fatigue lifetime, and then find the best compromise in terms of nitriding parameters. In order to determine the upper bound of profiles, each mechanical

property profile is determined independently from the other one. For instance, the required residual stress in-depth profile is calculated by assuming a constant hardness value through the nitrided surface and equal to the core hardness. In the opposite, the required hardness profile is determined assuming no residual stresses after nitriding. The two mechanical properties are then optimized both together according to the methodology presented in Figure 1 in order to take into account these two influences. The residual stress and hardness profiles are modified by dichotomy so as to obtain optimized profiles. The diagram summarizing all the steps is given in Figure 13.

4.2. Example

An example is given in Figure 14 for a given loading defined by an Hertz pressure of 4000 MPa between two cylinders of 5 mm spokes. The elements of the applied stress tensor are given by the equations of McEwen [17]. The durability is equal to 10^7 cycles, the probability of failure to 10^{-7}% and the core hardness to 400 HV0,2.

As illustrated in Figure 14, the calculated profiles are boundaries between rupture and non-rupture zones. To improve the mechanical properties for the given loading, compressive residual stresses and hardness must be sustained up to 300 μm. Compressive residual stresses of the order of -150 MPa are required to avoid crack initiation at the extreme surface due to the Hertz pressure on the surface. Tensile stresses due to the rebalancing in sublayers may theoretically be permitted, but must be limited, and even more avoided, such that rupture is prevented. On the other hand, in order to complete the benefit of nitriding process, the hardness must be higher than 590 HV0,2 close to the outter surface.

Thanks to the minimum requirement of residual stress and hardness as calculated for a given loading (Figure 14), the mechanical properties obtained for given nitriding parameters (Figur 12) can be validated as given in Figure 15.

In the case of a loading defined by a Hertz pressure of 4000 MPa, the residual stress and hardness located at the extreme surface are sufficient for all nitriding temperatures. However, the case depth obtained at a nitriding temperature of 520°C is similar to the minimum requirement. Consequently, the temperature must be greater than 520°C for a nitriding time of 30 h in order to avoid crack initiation.

In addition, the comparison of the profiles allows to obtain additional information on the probable zone of the crack initiation. For this example,

there is a high probability of rupture at the end of the nitrided layer for a temperature lower than 520°C. In fact, the profiles of hardness and residual stresses obtained or these nitriding parameters may lie in the breaking zone for a depth of between 100 and 300 μm.

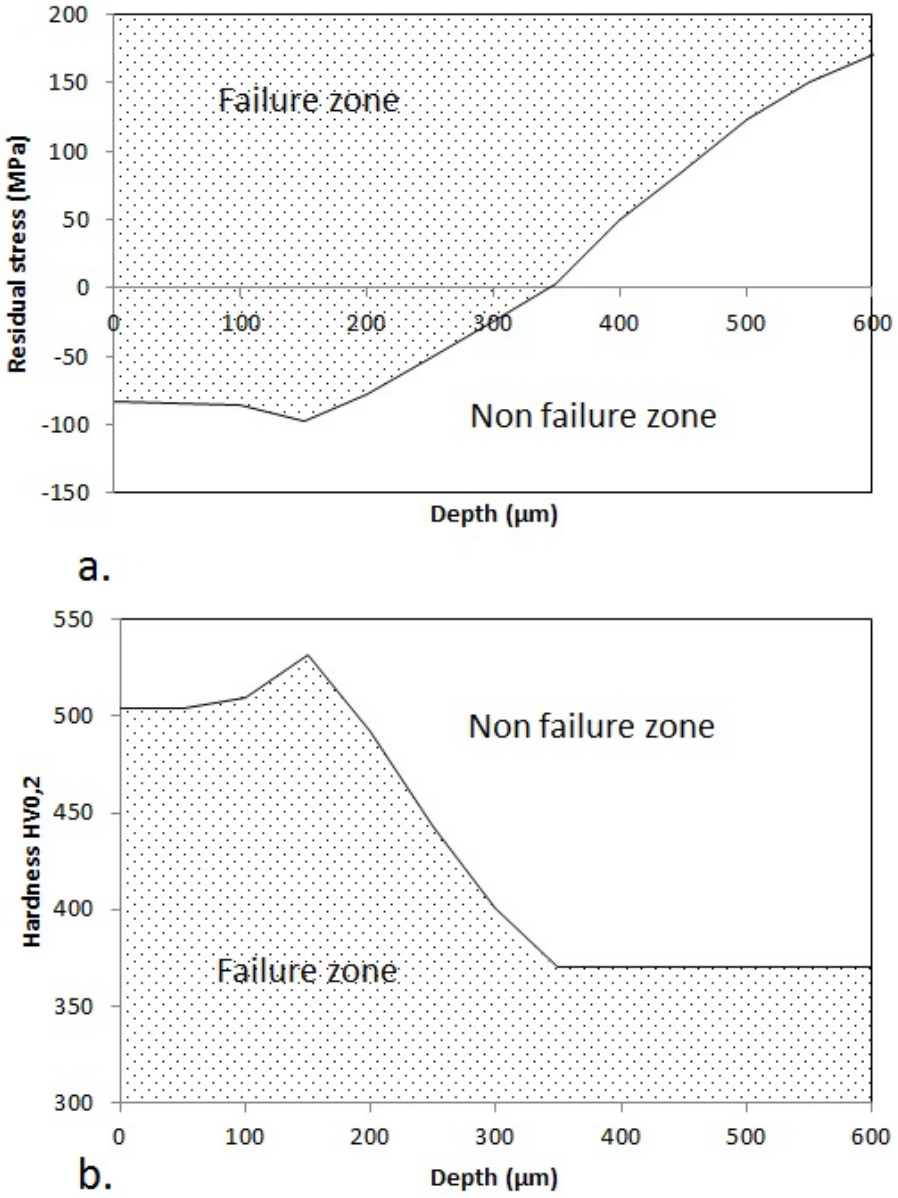

FIGURE 14: Theoretical residual stress (a.) and hardness (b.) in-depth profiles based on the Dang Van's criterion for 10^7 cycles and a 10^{-7} % probability of failure for a flank gear tooth.

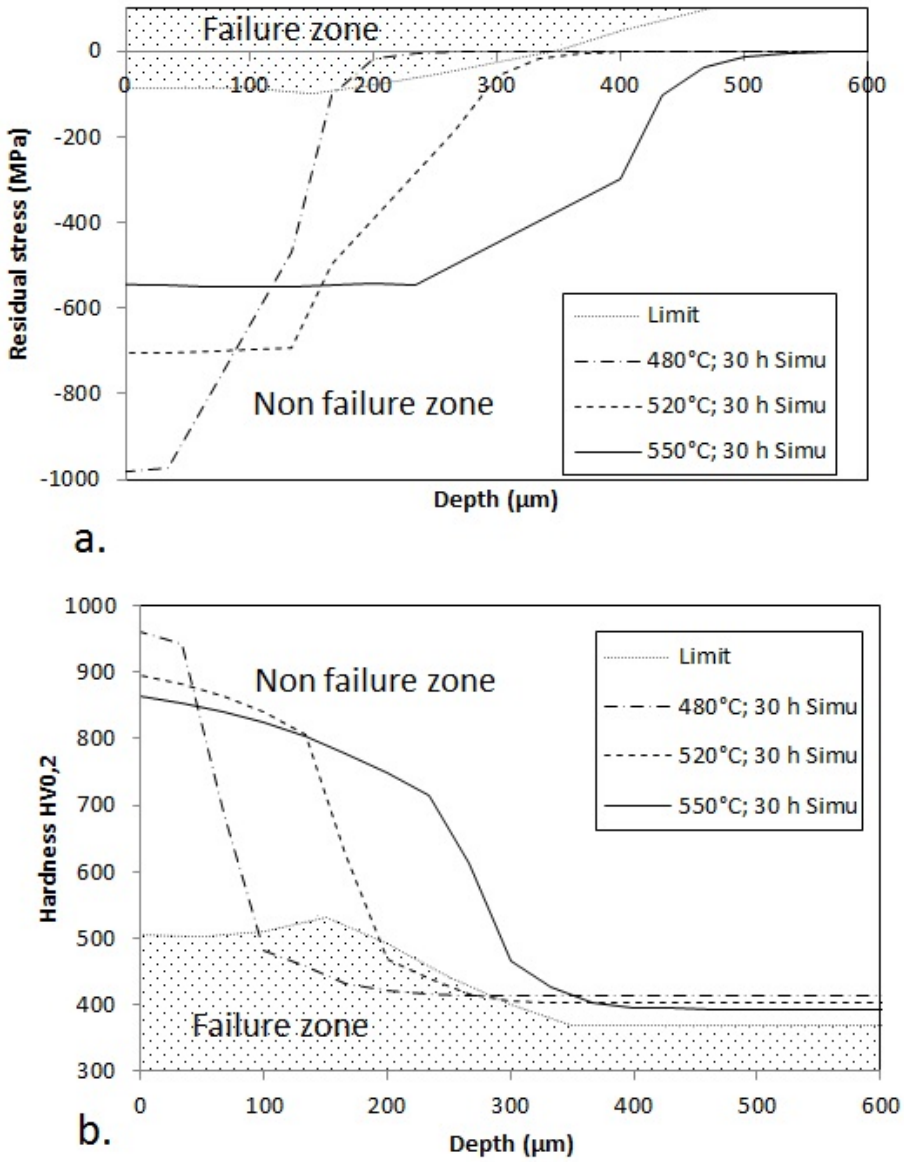

FIGURE 15: Comparison between minimum requirement of residual stress a) and hardness b) and the profiles obtained by simulation for 30-hour nitriding at 480, 520 and 550°C.

The optimization methodology by taking into account the residual stresses and hardness profiles is done by a dichotomy. It allows a good distribution between the hardness and residual stresses limit profiles. However, the results obtained are one possibility among others. The optimization of the nitriding

parameters depends on the methodology used. The dichotomy is in line with the gas nitriding process, since it provides limits profiles reflecting the influence of residual stresses and hardness.

Another form of optimization can be chosen by taking into account the influence of the residual stresses or hardness. This kind of method could be used for surface treatment with only one mechanical properties but it will not be appropriate in our case.

5. Conclusion

The optimization of the nitriding parameters (temperature, time) for a given fatigue lifetime, probability of failure and loading can be performed using two complementary steps :

- The multiaxial fatigue criteria like Dang Van, can be used in order to take into account the residual stress and hardness provided by the nitriding process. The implementation of Dang Van's criteria in an algorithm allows to calculate a minimum requirement of hardness and residual stress profiles to prevent failure of the nitrided workpiece.
- The residual stress and hardness profiles are obtained by the modelling of gas nitriding.

With this complete inverse method developed in this study, coupling material and mechanical simulation, the optimization of the nitriding can be performed for low alloys steels. This approach can be improved by :

- the kinetic aspect allowing to follow the evolution of the microstructure during nitriding was not developed during this study. This would have brought more precision to calculations of hardness and residual stresses.
- Additional contact fatigue tests would allow us to deepen and confirm the use of multiaxial fatigue criteria in this specific area.
- it would be interesting to extend the study in order to better understand the influence of the microstructure on the initiation of crack within a nitrided layer.

By means of comparison, it is now possible to validate the hardness and residual stress profiles obtained by modeling the nitriding process for a given nitriding cycle, a lifetime, a load and a given failure probability. Indeed, the nitriding cycle will not be validated if the limit profile is crossed by the simulated profile and the latter is in the rupture zone. In addition, the

comparison of the profiles makes it possible to obtain additional information on the probable zone of the initiation of rupture.

[1] K. H. Jack. *Nitriding*, volume 4. 1973.

[2] E. J. Mittemeijer. Die beziehung zwischen makro und mikroeigenspannungen. *Haerterei-Technische Mitteilungen*, 39 :16–29, 1984.

[3] L. Castex, J. Barralis, and J. C. Chaize. Etude de la tenue en fatigue de l'acier 32cdv13 nitruré. *Mémoires et études scientifiques revue de métallurgie*, 168 :13–23, 1987.

[4] D. H. Jack and S. Winnik. Effect of process variables on the fatigue resistance of nitrided steel. *Heat Treament*, pages 169–177, 1979.

[5] D. Girodin. Deep nitrided 32crmov13 steel for aerospace bearings applications. *NTN Technical review*, 76 :24–31, 2008.

[6] L. Barrallier. *Genèse des contraintes résiduelles de nitruration - Etude expérimentale et modélisation.* PhD thesis, ENSAM, Aix-en-Provence, 1992.

[7] S. Jégou, L. Barrallier, and R. Kubler. Phase transformations and induced volume changes in a nitride ternary fe-3 *Acta Materialia*, 58 :2666–2676, 2010.

[8] S. Jégou, L. Barrallier, R. Kubler, and M. A. J. Somers. Evolution of residual stress in the diffusion zone of a model fe-cr-c alloy during nitriding. *HTM J. Heat Treatm. Mat.*, 66 :135–142, 2011.

[9] S. Jégou, L. Barrallier, and G. Fallot. Opitimization of gaseous nitriding of steels by multi-physics modelling. *23 International Federation of Heat Treatment and Surface Engineering Congress 2016*, pages 63–70, 2016.

[10] V. Hruby V. Horàk and T. Mràskovà. Model for predicting microhardness profiles of steel after nitriding. *Advances in Military Technology*, 8 :5–12, 2013.

[11] Y. Watanabe Y. Hiraoka and O. Umezawa. Practical model to predict diffusion layer's hardness profile in gas nitrided low alloy steel containing chromium. *J. Japan Inst. Met. Mater.*, 80 :259–267, 2016.

[12] M. Chaussumier. *Un modèle statistique de calcul en fatigue multiaxiale pour les pièces mécaniques en acier nitruré.* PhD thesis, ENSAM, Aix-en-Provence, 2000.

[13] O. Message K. Dang Van, B. Griveau. On a new multiaxial fatigue criterion : theory and application. biaxial and multiaxial fatigue. *Mechanical Engineering Publications*, pages 479–496, 1989.

[14] R. Fathallah, A. Laamouri, H. Sidhom, and C. Braham. High cycle fatigue behavior prediction of shot-peened part. *International Journal of Fatigue*, 26 :1053–1067, 2004.

[15] M.A. Terres, S. Ben Mohamed, and H. Sidhom. Influence of ion nitriding on fatigue strength of low-alloy (42crmo4) steel : Experimental characterization and predictive approach. *International Journal of Fatigue*, 32 :1795–1804, 2010.

[16] A. Deperrois. *Sur le calcul de limite d'endurance des aciers.* PhD thesis, Ecole Polytechnique, 1991.

[17] E. McEwen. Stresses in elastic cylinders in contact along a generatrix. *Philosophical Magazine*, 40, 1949.

[18] *Thermo-calc software tcfe7 steel/fe-alloys database version 7.0.* 2013.

[19] L. Barrallier. *Thermochemical Surface Engineering of Steels : Improving Materials Performance.* Metals and Surface Engineering, 2014.

[20] T. Mura. *Micromechanics of defects in solids.* Martinus Nijhoff Publishers, 1987.

[21] A. Zaoui D. François, A. Pineau. *Comportement Mécanique des Matériaux : Elasticité et plasticité.* Hermès, 1995.

[22] L. M. Brown and R. K. Ham. *Strenghtening Methods in crystals.* Ed. A. Kelly and R.B.Nicholson, 1971.

[23] E. Orowan. *Discussion in the symposium on Internal Stresses in Metals and Alloys.*, volume 3. Inst. Metals, 1948.

[24] P. Guyot. Hardening by ordered coherent precipitates related to the statistical theory. *Phil. Mag.*, 24 :987–993, 1971.

[25] G. Fallot. *Rôle du carbone lors de la nitruration d'aciers de construction et influence sur les propriétés mécaniques.* PhD thesis, ENSAM, Aix-en-Provence, 2015.